Photochemical & Photobiological Sciences

Accepted Manuscript

This is an *Accepted Manuscript*, which has been through the Royal Society of Chemistry peer review process and has been accepted for publication.

Accepted Manuscripts are published online shortly after acceptance, before technical editing, formatting and proof reading. Using this free service, authors can make their results available to the community, in citable form, before we publish the edited article. We will replace this *Accepted Manuscript* with the edited and formatted *Advance Article* as soon as it is available.

You can find more information about *Accepted Manuscripts* in the Information for Authors.

Please note that technical editing may introduce minor changes to the text and/or graphics, which may alter content. The journal's standard Terms & Conditions and the Ethical guidelines still apply. In no event shall the Royal Society of Chemistry be held responsible for any errors or omissions in this *Accepted Manuscript* or any consequences arising from the use of any information it contains.

ROYAL SOCIETY OF CHEMISTRY

www.rsc.org/pps

Photochemical & Photobiological Sciences RSCPublishing

ARTICLE

A New Antitumoral Heteroarylaminothieno[3,2-*b*]pyridine Derivative: Incorporation in Liposomes and Interaction with Proteins Monitored by Fluorescence

Cite this: DOI: 10.1039/xoxxoooooox

Received ooth July 2014,
Accepted ooth January 2012

DOI: 10.1039/xoxxoooooox

www.rsc.org/

C. N. C. Costa[a], A. C. L. Hortelão[a], J. M. F. Ramos[a], A. D. S. Oliveira[a], R. C. Calhelha[b], M.-J. R. P. Queiroz[b], P. J. G. Coutinho[a], E.M.S. Castanheira[a] †

[a] Centro de Física, Universidade do Minho (CFUM), Campus de Gualtar, 4710-057 Braga, Portugal.
[b] Centro de Química, Universidade do Minho (CQ/UM), Campus de Gualtar, 4710-057 Braga, Portugal.
† Corresponding author; Phone: +351 253604321; Fax: +351 253604061; ecoutinho@fisica.uminho.pt

The fluorescence properties of the new potent antitumoral methyl 3-amino-6-(benzo[*d*]thiazol-2-ylamino)thieno[3,2-*b*]pyridine-2-carboxylate in solution and when encapsulated in several different nanoliposome formulations were investigated. The compound exhibits very reasonable fluorescence quantum yields and a solvent sensitive emission in several polar and non-polar media, despite not being fluorescent in protic solvents.

Fluorescence anisotropy measurements of the compound incorporated in liposomes revealed that this thienopyridine derivative can be carried in the hydrophobic region of the lipid membrane. Liposome formulations including this antitumor compound are nanometric in size, with a diameter lower than 130 nm and generally low polydispersity, being promising for future drug delivery developments.

The interaction of the compound with bovine serum albumin (BSA) and the multidrug resistance protein MDR1 was monitored by FRET, the compound acting as energy acceptor. It was observed a lower interaction with MDR1 protein than with the native form of BSA, which is an important result regarding applications of this antitumoral drug.

Introduction

Thienopyridine derivatives have attracted much attention as they exhibit important biological activity, namely as antitumoral agents,[1-5] nonreceptor Src kinase inhibitors,[6] receptor tyrosine kinase[7] and vascular endothelial growth factor (VEGFR-2) inhibitors,[8-9] the latter related to angiogenesis and metastasis.

The methyl 3-amino-6-(benzo[*d*]thiazol-2-ylamino)-thieno[3,2-*b*]pyridine-2-carboxylate (**1**) (Figure 1) was previously synthetized by us by palladium-catalysed C-N Buchwald-Hartwig coupling.[2] Compound **1** showed to be the most potent antitumor compound among a series of synthesized methyl 3-amino-6-[(hetero)arylamino]thieno[3,2-*b*]pyridine-2-carboxylates, presenting very low growth inhibitory concentration values (GI_{50}) between 3.5 and 6.9 μM, when tested in vitro (with a 24h incubation time and using DMSO as solvent) against several human tumour cell lines, MCF-7 (breast adenocarcinoma), A375-C5 (melanoma) and NCI-H460 (non-small cell lung cancer).[2]

Due to this potent antitumor activity of compound **1**, which is the most active of a series of analogues,[2] its behaviour in liposomes and when interacting with both plasma and membrane proteins is of particular interest, considering future developments using this thienopyridine derivative as an antitumoral drug.

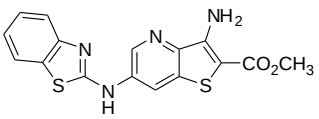

Compound **1**

Fig. 1 Structure of the methyl 3-amino-6-(benzo[*d*]thiazol-2-ylamino)thieno[3,2-*b*]pyridine-2-carboxylate (**1**).

The multidrug resistance is one of the major gaps of many forms of chemotherapy, which can be associated with an overexpression of drug pumps. These pumps are usually membrane proteins and the study of drug interaction with such proteins may be useful for reversing drug resistance in cancer.[10] Multidrug transport proteins can actively remove toxic compounds and are of fundamental importance in the resistance to both antibiotics and anticancer drugs.[11,12]

The interaction with human and bovine serum albumins (HSA and BSA, respectively) has also been extensively studied

for several drugs, among others for efonidipine (an antihypertensive and antianginal agent),[13] quercetin (flavonoid antioxidant agent),[14] ceftriaxone (antibiotic),[15] alprazolam (psychotropic drug)[16] and anastrozole (anticancer drug).[17] In particular, BSA is used as a model for HSA as, upon sequence alignment, they share about 76% of the amino acid sequence identity. Serum albumin, while being responsible for the osmotic pressure of the blood (among other key roles), acts as vehicle for long chain fatty acids, vitamins, amino acids, hormones, some metal ions (Zn^{2+}, Cu^{2+}) and drugs like penicillins and benzodiazepines.[18-21] In this work, we investigate whether BSA is able to bind and carry compound **1** in the blood stream.

Nanoliposomes are promising systems in drug delivery and their stability and efficiency is strongly related with their composition.[22,23] Considering the very low solubility of compound **1** in aqueous media, the use of liposomes as transport vehicles is of special importance. Is has been reported that the presence of cholesterol may increase the stability of the lipid vesicles by preventing crystallization of the phospholipid acyl chains and providing steric hindrance to their movement, while also acting as modulator of the bilayer fluidity. Recently, the phospholipid DMPG has been widely employed in liposome formulations, as it provides the formation of pores across the lipid membrane[24] which has a promising biological relevance in controlled release from nanocompartments.[25] Advances in liposome research also found that PEG allows longer circulatory life of the drug delivery system, while being inert in the body.[26]

In this work, compound **1** was incorporated in several nanoliposome formulations, and its behaviour was studied by fluorescence. The interaction of this antitumoral drug with the plasma protein BSA and the multidrug resistance protein MDR1 was evaluated by FRET (Förster Resonance Energy Transfer).

Experimental

Materials and Methods

All the solutions were prepared using spectroscopic grade solvents and ultrapure water (Milli-Q grade). The proteins Bovine Serum Albumin (lyophilized powder) and human MDR1 (membrane preparation expressed in S*f9* cells) were obtained from Sigma-Aldrich.

Buffers with pH values of 2, 5 and 7 were prepared according to a standard procedure,[27] using a mixed solution of 0.2 M boric acid and 0.05 M citric acid and a 0.1 M solution of sodium phosphate.

1,2-Dipalmitoyl-*sn*-glycero-3-phosphocholine (DPPC), 1,2-diacyl-*sn*-glycero-3-phosphocholine from egg yolk (Egg-PC), 1,2-dipalmitoyl-*sn*-glycero-3-[phospho-*rac*-(1-glycerol)] (sodium salt) (DPPG), 1,2-dimyristoyl-*sn*-glycero-3-[phospho-*rac*-(1-glycerol)] (sodium salt) (DMPG) and cholesterol (Ch) were obtained from Sigma-Aldrich. 1,2-Distearoyl-*sn*-glycero-3-phosphoethanolamine-*N*-[methoxy(polyethylene glycol)-2000] (ammonium salt) (DSPE-PEG) was obtained from Avanti Polar Lipids, while dioctadecyldimethylammonium bromide (DODAB) was purchased from Tokyo Kasei. Lipid structures are shown in Figure 2.

For Egg-PC membranes preparation, defined volumes of stock solutions of lipid and compound in ethanol were injected together, under vigorous stirring, to an aqueous buffer solution (10 mM Tris-HCl buffer, pH=7.4), at room temperature (ethanolic injection method[28,29]). A similar procedure was adopted for the other lipid membranes and lipid formulations, but the injection of the required amounts of stock solutions of lipid and compound in ethanol were done at 60 ˚C, well above the lipids melting transition temperature (41 ºC for DPPC,[30] 40 ºC for DPPG,[31] 23 ºC for DMPG[32] and 45 ºC for DODAB[33]), followed by six extrusion cycles (using a LIPEX^{TM} extruder) through 100 nm polycarbonate membranes. Extrusion technique was used to diminish the mean diameter and polydispersity of the liposomes, making them suitable for nanoscale delivery. Between the extrusion cycles, the solutions were allowed to equilibrate for 1 hour. The final total lipid concentration was 1 mM, with a compound/lipid molar ratio of 1:500. Fluorescence measurements in liposomes were performed using samples prepared with this same protocol.

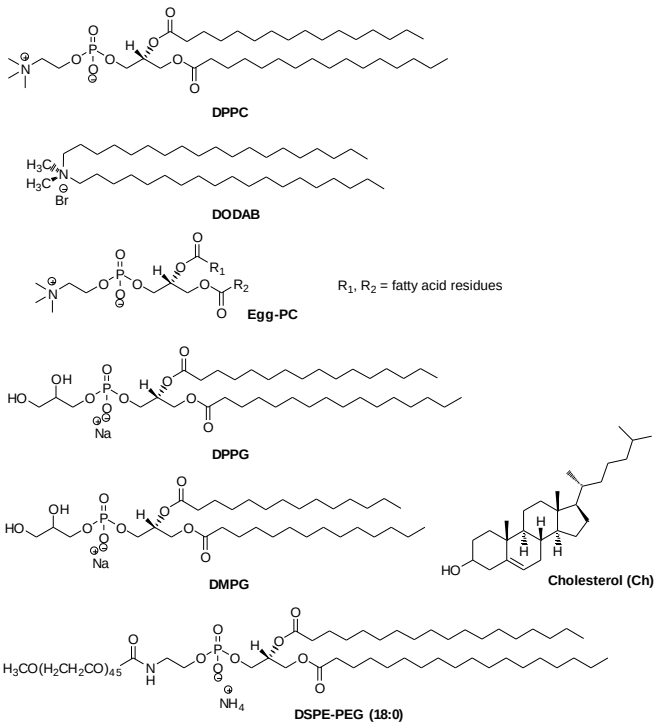

Fig. 2 Structures of the lipids used in nanoliposomes formulations.

DLS measurements

Liposomes mean diameter and size distribution (polydispersity index) were measured using a Dynamic Light Scattering (DLS) equipment (NANO ZS Malvern Zetasizer), at 25 ºC, using a He-Ne laser of 633 nm and a detector angle of 173º. Five independent measurements were performed for each sample. Malvern Dispersion Technology Software (DTS) was used with multiple narrow mode (high resolution) data processing, and mean size (nm) and error values were considered.

Spectroscopic measurements

General methods. Absorption spectra were recorded in a Shimadzu UV-3101 PC UV-Vis-NIR spectrophotometer. Fluorescence measurements were performed using a Fluorolog 3 spectrofluorimeter, equipped with double monochromators in both

excitation and emission, Glan-Thompson polarizers and a temperature controlled cuvette holder.
For fluorescence quantum yield determination, the solutions were previously bubbled for 30 minutes with ultrapure nitrogen. Fluorescence spectra were corrected for the instrumental response of the system.

The fluorescence quantum yields (Φ_S) were determined using the standard method (equation 1).[34,35] The IUPAC recommendations for this method were followed.[36] Quinine sulfate in 0.05 M sulfuric acid was used as reference, $\Phi_r = 0.546$ at 25 ºC.[37]

$$\Phi_s = \left[\left(A_r F_s n_s^2\right)/\left(A_s F_r n_r^2\right)\right]\Phi_r \quad (1)$$

where A is the absorbance at the excitation wavelength, F the integrated emission area and n is the refraction index of the solvents. Subscripts refer to the reference (r) or sample (s) compound. The absorbance value at excitation wavelength was always less than 0.1, in order to avoid inner filter effects.

The Lippert-Mataga equation (equation 2), where the energy difference between absorption and emission maxima is related to the polarizability of the solvent,[38,39] was used to describe the solvatochromic shifts of compound **1**,

$$\bar{\nu}_{abs} - \bar{\nu}_{fl} = \frac{1}{4\pi\varepsilon_0}\frac{2\Delta\mu^2}{hcR^3}\Delta f + const \quad (2)$$

where $\bar{\nu}_{abs}$ is the wavenumber of maximum absorption, $\bar{\nu}_{fl}$ is the wavenumber of maximum emission, $\Delta\mu = \mu_e - \mu_g$ is the difference in the dipole moment of solute molecule between excited (μ_e) and ground (μ_g) states, R is the cavity radius, and Δf is the polarizability of the solvent, given by (equation 3):

$$\Delta f = \frac{\varepsilon - 1}{2\varepsilon + 1} - \frac{n^2 - 1}{2n^2 + 1} \quad , \quad (3)$$

where ε is the static dielectric constant and n the refractive index of the solvent.

The steady-state fluorescence anisotropy, r, is calculated by

$$r = \frac{I_{VV} - G I_{VH}}{I_{VV} + 2G I_{VH}} \quad (4)$$

where I_{VV} and I_{VH} are the intensities of the emission spectra obtained with vertical and horizontal polarization, respectively (for vertically polarized excitation light), and $G = I_{HV}/I_{HH}$ is the instrument correction factor, where I_{HV} and I_{HH} are the emission intensities obtained with vertical and horizontal polarization (for horizontally polarized excitation light).

FRET measurements. The interaction of compound **1** with proteins was evaluated by Förster Resonance Energy Transfer (FRET). For these experiments, the compound was dissolved in ethanol and injected in each protein solution.
FRET efficiency, Φ_{RET}, defined as the proportion of donor molecules that have transferred their excess energy to acceptor molecules, was calculated through donor emission quenching, by taking the ratio of the donor integrated fluorescence intensities in the presence of acceptor (F_{DA}) and in the absence of acceptor (F_D) (equation 5).[40]

$$\Phi_{RET} = 1 - \frac{F_{DA}}{F_D} \quad (5)$$

The distance between donor and acceptor molecules can be determined through the FRET efficiency (equation 6),

$$r_{AD} = R_0 \cdot \left[\frac{1-\Phi_{RET}}{\Phi_{RET}}\right]^{1/6} \quad (6)$$

where R_0 is the Förster radius (critical distance), that can be obtained by the spectral overlap, J(λ), between the donor emission and the acceptor absorption, according to equations (7) and (8) (with R_0 in Å, λ in nm, $\varepsilon_A(\lambda)$ in M^{-1} cm^{-1}),[40]

$$R_0 = 0.2108\left[k^2 \Phi_D^0 n^{-4} J(\lambda)\right]^{1/6} \quad (7)$$

$$J(\lambda) = \int_0^\infty I_D(\lambda)\varepsilon_A(\lambda)\lambda^4 d\lambda \quad (8)$$

where $k^2 = 2/3$ is the orientational factor assuming random orientation of the dyes, Φ_D^0 is the fluorescence quantum yield of the donor in the absence of energy transfer, n is the refraction index of the medium, $I_D(\lambda)$ is the fluorescence spectrum of the donor normalized so that $\int_0^\infty I_D(\lambda)d\lambda = 1$, and $\varepsilon_A(\lambda)$ is the molar absorption coefficient of the acceptor.

Results and Discussion

Photophysical properties in solution

The promising antitumoral properties of the thienopyridine **1** (Figure 1) inspired us to study the photophysical behaviour of this fluorescent compound in solution, as it is important for the understanding of compound interaction with proteins and liposomes. Therefore, the absorption and fluorescence properties of the thienopyridine derivative **1** were studied in several solvents of different polarity. The maximum absorption (λ_{abs}) and emission wavelengths (λ_{em}), molar absorption coefficients and fluorescence quantum yields of this compound are shown in Table 1. The normalized fluorescence spectra are shown in Figure 3 (examples of absorption spectra are displayed as insets).

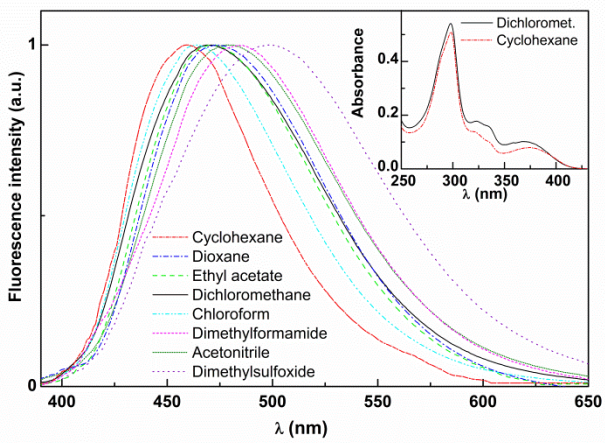

Fig. 3 Normalized fluorescence spectra (λ_{exc}=360 nm) of 3×10^{-6} M solutions of compound **1** in several solvents. Inset: Absorption spectra of 2×10^{-5} M solutions of compound in dichloromethane and cyclohexane, as examples.

Compound **1** presents moderate absorption coefficient values ($\varepsilon \geq 3\times10^3$ M^{-1} cm^{-1}) in all solvents (at the lowest energy absorption maximum) and also exhibits reasonable fluorescence quantum yields (Table 1). This behaviour in absorption and emission is common to other thienopyridine derivatives previously studied,[41-43] and was attributed to a state mixing between a $\pi\rightarrow\pi^*$ transition (aromatic ring system) and a $n\rightarrow\pi^*$ transition (carbonyl group).[44]

Compound **1** is not fluorescent in protic solvents, pointing to hydrogen bond formation with this kind of solvents, or by protonation of the N atom of the pyridine ring, as already reported by us for methoxylated di(hetero)arylethers in the thieno[3,2-*b*]pyridine series[41] and for 1,3-diarylureas linked to methyl 3-aminothieno[3,2-*b*]pyridine-2-carboxylate moiety.[42] Also a common feature is the significant red shifts observed for emission in polar solvents (32 nm between cyclohexane and dimethylsulfoxide) (Figure 3), usually attributed to an intramolecular charge transfer (ICT) mechanism or to specific solvent effects,[38] indicating a major role for solvent relaxation after photoexcitation.

The solvatochromic shifts were plotted using the Lippert-Mataga equation (equation 2, Figure 4). This plot is reasonably linear and the high slope value allows concluding that compound **1** has a pronounced ICT character in the excited state.

With Gaussian 09 software[46] and use of a 6-311+G(dp) basis set at the TD-SCF DFT (MPW1PW91) level of theory[47] in gas phase, the optimized geometries of the ground and the first excited singlet states were obtained (Figure 5), showing that the ring systems are completely planar. The blue arrows indicate the direction of the calculated dipole moments, pointing to a change in direction of the excited state dipole moment relative to the ground state. Absolute values of dipole moments, μ_g=3.53 D and μ_e=4.46 D, and a cavity radius of R=5.53 Å were estimated by Gaussian calculations. Using the vectors coordinates, the magnitude of dipole moment difference, $|\vec{\mu}_e - \vec{\mu}_g|$= 6.47 D, is lower than the predicted from the Lippert-Mataga solvatochromic plot (Figure 4), $|\vec{\mu}_e - \vec{\mu}_g|$= 8.96 D, as the latter does not include the change in the vector direction.

Table 1. Maximum absorption (λ_{abs}) and emission (λ_{em}) wavelengths, molar absorption coefficients (ε) and fluorescence quantum yields (Φ_F) for the thieno[3,2-*b*]pyridine derivative **1** in several solvents.

Solvent	λ_{abs} (nm) (ε /10^4 M^{-1} cm^{-1})	λ_{em} (nm)	Φ_F [a]
Cyclohexane	374 (0.39); 298 (2.55); 235 (1.57)	460	0.43
Dioxane	372 (0.48); 299 (2.34); 237 (1.71)	472	0.40
Chloroform[b]	368 (0.51); 299 (2.74)	464	0.14
Ethyl acetate[b]	369 (0.52); 322 (0.88); 298 (2.66)	470	0.17
Dichloromethane	367 (0.51); 323 (0.89); 298 (2.71); 235 (1.79)	469	0.22
Dimethylsulfoxide[b]	369 (0.91); 341 (1.23)	492	0.32
N,*N*-Dimethylformamide[b]	367 (1.09); 342 (1.53); 290 (3.34)	484	0.23
Acetonitrile	362 (0.60); 324 (0.91); 296 (2.47); 235 (1.75)	478	0.14
Ethanol	365 (0.63); 325 (0.93); 299 (2.24)	---	---
Methanol	365 (0.61); 324 (0.94); 298 (2.29)	---	---
Water	366 (0.31); 324 (0.63); 299 (1.28)	---	---

[a] Relative to quinine sulfate in 0.05M sulfuric acid (Φ_r =0.546).[37] Error about 10%.
[b] Solvents *cut-off:* chloroform: 250 nm; ethyl acetate: 265 nm; dimethylsulfoxide: 270 nm; *N*,*N*-dimethylformamide: 275 nm.

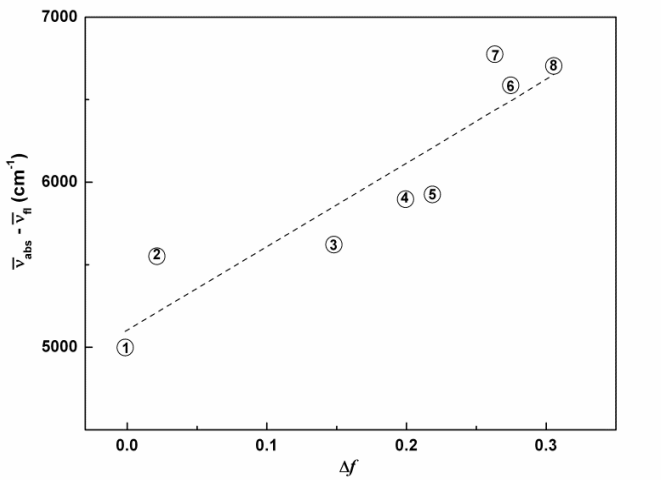

Fig. 4 Lippert-Mataga plot for compound **1**. Solvents: 1 – cyclohexane; 2 – dioxane; 3 – chloroform; 4 – ethyl acetate; 5 – dichloromethane; 6 – dimethylsulfoxide; 7 – *N*,*N*-dimethylformamide; 8 – acetonitrile (values of ε and n were obtained from ref. 45).

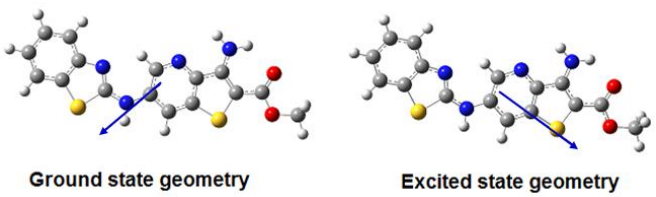

Fig. 5 Optimized geometries for compound **1** calculated by Gaussian 09 software (grey: C atoms; white: H atoms; red: O atoms; blue: N atoms; yellow: S atoms). Left: ground state; Right: lowest excited singlet state. The arrows indicate the direction of the dipole moment.

The representation of the electronic density difference between the lowest excited state and ground state is displayed in Figure 6A, as well as the corresponding centroids of either the electronic depletion (C_+) or increment (C_-)[48] that occurs upon electronic excitation, using the lowest excited state optimized geometry (relaxed S_1 state) (Figure 6B).

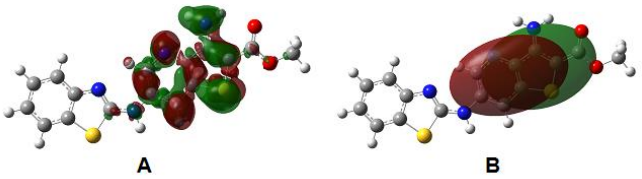

Fig. 6 A. Electronic density difference (optimized geometry for the lowest excited singlet state) at an *iso* level of 0.001; green regions: loss of electronic density; red regions: enrichment of electronic density. **B**. Centroids of electronic charge density depletion (C_+, green) or increment (C_-, red) at the same *iso* level.

The electron density variations occur mostly on the thieno[3,2-*b*]pyridine moiety, which is a common behavior with other thieno[3,2-*b*]pyridine derivatives already synthesized by some of us, namely 1,3-diaylurea derivatives[42] and 6-(hetero)arylthieno[3,2-*b*]pyridines.[43] The charge transfer character of the excited state is confirmed by the electron density transfer from the amino group linked to the thiophene ring of thienopyridine moiety and its sulfur atom to the pyridine moiety (Figure 6A). The distance of 1.82 Å between the barycenters of charge density also supports the charge transfer character. The calculations of densities of charge increase and depletion (figure 6B) were performed with the help of the Multiwfn software package.[49]

The significant sensitivity of the fluorescence emission of compound **1** to its environment can be useful when probing the location/behavior of this antitumoral thienopyridine derivative in liposomes of several compositions.

Incorporation of compound 1 in nanoliposomes

The thienopyridine derivative **1** was encapsulated in liposomes of different compositions, either composed of neat lipids or lipid formulations based on previous work, including cholesterol and PEG.[30,43,50] The influence of the surface charge was investigated, using zwitterionic phospholipids (the phosphatidylcholines Egg-PC and DPPC), anionic lipids (DPPG, DMPG) and a cationic synthetic amphiphile (DODAB).

DLS measurements. In order to obtain information about the more promising liposome formulations for the incorporation of compound **1**, the mean size and size distribution (polydispersity, PdI) of the nanoliposome formulations containing this compound were determined by Dynamic Light Scattering (DLS) (Table 2). This is especially important considering the emerging nanoscale delivery systems using liposomes for the delivery of drugs in disease treatment.[22]

DLS measurements indicate that all the nanoliposomes tested with the incorporated compound **1** have low polydispersity (PdI < 0.4) and with hydrodynamic diameters between 60 and 125 nm. As previously reported for other thienopyridine derivatives,[41,43] the formulations based in Egg-PC have generally the smallest sizes and low polydispersity. It can also be observed that the inclusion of DMPG causes a diminution in size of liposomes containing 50% DMPG or above, with diameters lower than 100 nm (Table 2). PEGylation induces a small increase in particle diameter with a decrease in polydispersity (Table 2). On the other hand, the more polydisperse formulations are the ones rich in DPPC (DPPC:Ch 7:3 and DPPC:DMPG 2:1).

Table 2. Hydrodynamic diameter and polydispersity of several liposome formulations containing the thienopyridine derivative **1**, at 25 ºC.

Formulation	Hydrodynamic diameter (nm) (mean ± SD)	Polydispersity (mean ± SD)
Egg-PC:Ch (7:3)	84 ± 2	0.233 ± 0.004
Egg-PC:Ch:DMPG (7:3:1)	63.7 ± 0.4	0.284 ± 0.003
DPPC:DMPG (1:1)	99 ± 3	0.33 ± 0.04
DPPC:DMPG (2:1)	124 ± 1	0.38 ±0.07
DPPC:DMPG (1:2)	91 ± 1	0.23 ± 0.01
DPPC:Ch (7:3)	110 ± 3	0.38 ± 0.08
DPPC:Ch:DSPE-PEG (7:3:1)	117 ± 1	0.27 ± 0.01

Standard deviations (SD) were calculated from the mean of the data of a series of five experiments conducted using the same parameters.

Fluorescence measurements. Fluorescence emission spectra of the thienopyridine derivative **1** in liposomes were measured in both gel (below the melting temperature, T_m) and liquid-crystalline (above T_m) phases of each lipid. The lipids DPPC, DPPG and DODAB are in the gel phase at room temperature, while the egg phosphatidylcholine is in the fluid phase (T_m is very low for this phosphatidylcholines mixture[51]). The spectra are shown in Figure 7 (maximum emission wavelengths are presented in Table 3).

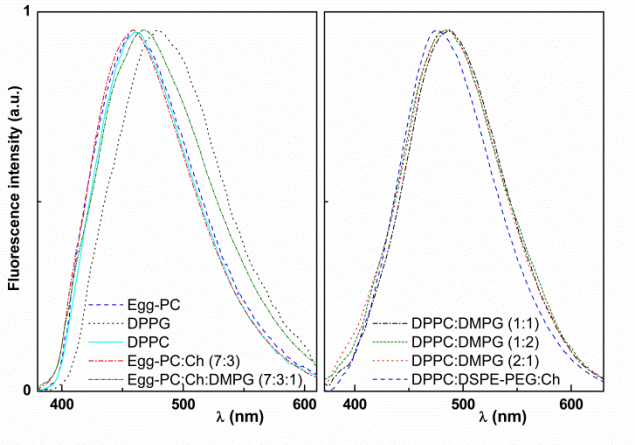

Fig. 7 Normalized fluorescence spectra of compound **1** (3×10^{-6} M) in liposomes of several compositions, at room temperature (λ_{exc} = 360 nm).

Relevant information about the location/behavior of this antitumoral compound in liposomes can be obtained through fluorescence anisotropy (*r*) measurements, as the *r* value increases with the rotational correlation time of the fluorescent molecule (and, thus, with the viscosity of the environment, equation 9)[40]

$$\frac{1}{r} = \frac{1}{r_0}\left(1+\frac{\tau}{\tau_c}\right) \quad (9)$$

where r_0 is the fundamental anisotropy, τ is the excited-state lifetime and τ_c is the rotational correlation time.

The fluorescence (steady-state) anisotropies of this thienopyridine derivative in the several liposomes are shown in Table 3. For comparison, the fluorescence anisotropy in glycerol (a very viscous solvent, η=993.4 cP at 25 ºC [45]) at room temperature was also determined (r = 0.327). An increase of the steady-state anisotropy is expected from a diminution of the excited-state lifetime (equation 9). Upon temperature increase, the excited-state lifetime is predicted to decrease, due to the increment of the non-radiative deactivation pathways, especially the rate constant for internal conversion $S_1 \rightarrow S_0$. As the anisotropy value decreases strongly at higher temperature (Table 3), this behavior can be attributed to a decrease of the rotational correlation time of the fluorophore. This originates from the decrease of membrane microviscosity upon changing from the gel to the liquid-crystalline phase of the lipids DPPC (T_m=41 ºC),[30] DPPG (T_m=40 ºC)[31] and DODAB (T_m=45 ºC).[33]

Table 3. Steady-state fluorescence anisotropy (r) values and maximum emission wavelengths (λ_{em}) for compound **1** in several liposome formulations, at 25 ºC and 55 ºC.

Lipid formulation	Temp.	λ_{em} (nm)	r
Egg-PC (100%)	25 ºC	459	0.176
DPPC (100%)	25 ºC	460	0.256
	55 ºC	458	0.130
DPPG (100%)	25 ºC	479	0.186
	55 ºC	477	0.129
DODAB (100%)	25 ºC	480	0.153
	55 ºC	479	0.071
Egg-PC:Ch (7:3)	25 ºC	458	0.137
Egg-PC:Ch:DMPG (7:3:1)	25 ºC	466	0.122
DPPC:Ch (7:3)	25 ºC	461	0.129
	55 ºC	459	0.102
DPPC:DMPG (1:1)	25 ºC	479	0.224
	55 ºC	477	0.084
DPPC:DMPG (2:1)	25 ºC	478	0.225
	55 ºC	476	0.093
DPPC:DMPG (1:2)	25 ºC	479	0.215
	55 ºC	478	0.074
DPPC:Ch:DSPE-PEG (7:3:1)	25 ºC	476	0.124
	55 ºC	474	0.104

To analyse and compare the steady-state fluorescence anisotropy values at room temperature (Table 3), the Strickler-Berg equation,[52] relating the radiative lifetime with the absorption intensity (equation 10) could be used

$$\frac{1}{\tau_r} = 2.88\times10^{-9} n^2 \frac{\int F_{\bar{\nu}}(\bar{\nu}_F)\mathrm{d}\bar{\nu}_F}{\int \bar{\nu}_F^{-3} F_{\bar{\nu}}(\bar{\nu}_F)\mathrm{d}\bar{\nu}_F} \int \frac{\varepsilon(\bar{\nu}_A)\mathrm{d}\bar{\nu}_A}{\bar{\nu}_A} \qquad (10)$$

where τ_r is the radiative lifetime, n is the index of refraction, ε is the molar absorption coefficient, and $F_{\bar{\nu}}(\bar{\nu}_F)$ is the fluorescence intensity per unit wavenumber. This quantity is related to the fluorescence quantum yield,[40] through

$$\int_{\infty}^{0} F_{\bar{\nu}}(\bar{\nu}_F)\mathrm{d}\bar{\nu}_F = \Phi_F \qquad (11)$$

Fluorescence quantum yields of compound **1** in neat liposomes were determined by the standard method[34,35] (equation 1) as Φ_F=0.11 in DPPC, Φ_F=0.08 in DPPG, Φ_F=0.07 in DODAB, and Φ_F=0.11 in Egg-PC. These values are roughly similar and, as the absorption spectra in the several liposomes are also analogous, the Stickler-Berg relation (equation 10) predicts an approximately constant value for the radiative lifetime in all the lipid vesicles.

The fluorescence quantum yield and the excited-state lifetime are related by equation 12,

$$\Phi_F = k_r \tau \qquad (12)$$

where $k_r = 1/\tau_r$ is the rate constant for radiative deactivation with fluorescence emission.[40] Taking this into account, we can conclude that the compound excited-state lifetime is approximately constant for the studied liposomes at 25 ºC. Therefore, variations in fluorescence anisotropy at room temperature can be directly related to changes in the rotational correlation time of the fluorescent compound and, thus, to changes in the microviscosity of its surrounding medium.

The differences in anisotropy values between the compound incorporated in the several lipid aggregates and in glycerol at room temperature can also be attributed to the distinct environment viscosities,[43] as glycerol is much more viscous than lipid membranes, which viscosity values are around 100-200 cP.[53,54]

In neat DPPG (anionic) and DODAB (cationic) aggregates, as well as in DMPG-containing formulations, the maximum emission wavelengths point to a more hydrated environment than in zwitterionic Egg-PC or DPPC aggregates (Table 3). Anisotropy values are also lower for neat DPPG and DODAB than for neat DPPC, indicating that an increased hydration also corresponds to an increased membrane fluidity where the compound molecules are located. The influence of the lipid charge seems to be negligible in compound behaviour, pointing to a main location in the beginning of the inner membrane, due to its hydrophobic character.

The influence of DMPG in the liposomes properties can be attributed to the ability of this phospholipid to create perforations in the lipid bilayers,[24,25] inducing also a more hydrated environment for the thienopyridine derivative in DMPG-rich systems. The effect of cholesterol (Ch) seems to be a rise in fluidity of the lipid membranes, as previously reported,[42,43] which can be inferred from the significant decrease in anisotropy at room temperature in Ch-containing systems. The presence of PEG does not influence compound anisotropy, which can be explained by a deep location of the fluorophore in the lipid membranes, while PEG usually covers the lipid aggregates.

Interaction with proteins

Considering the promising antitumoral properties of compound **1**, its interaction with proteins was also investigated. A plasma protein, Bovine Serum Albumin (BSA), and a membrane protein (human multidrug resistance MDR1) were employed in this study. The interaction was evaluated by FRET (Förster Resonance Energy

Transfer) from the protein amino acids tyrosine and tryptophan to the fluorescent compound **1**.

It is known that BSA protein has pH-dependent conformations, undergoing a transition from the extended form to the native form when pH increases from 2.7 to 4.3.[55] Therefore, these studies were performed at three different pH values (2, 5 and 7), as conformational changes can markedly influence the compound affinity to BSA. Figure 8 shows the spectral overlap between the fluorescence emission of proteins MDR1 and BSA, the latter in both the native (pH=7) and extended (pH=2) forms, and the absorption of compound **1**, evidencing the possibility of FRET between each protein (donor) and compound **1** (acceptor).

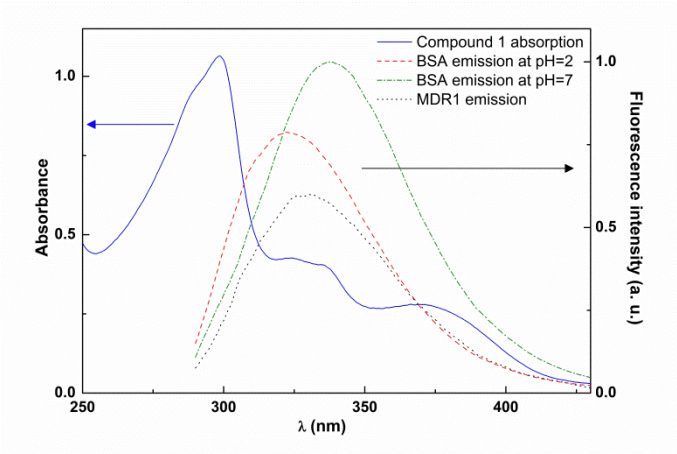

Fig. 8 Spectral overlap between the fluorescence emission of both MDR1 and BSA (at pH=2 and pH=7) and the absorption of compound **1**.

FRET measurements were performed at several protein/compound molar ratios, keeping constant compound concentration. Exciting in the region where proteins absorb, through the aromatic amino acids tyrosine and tryptophan (λ_{exc}=280 nm), it is possible to observe the fluorescence emission of compound (λ_{max}=450 nm) (Figures 9 and 10). At λ_{exc}=280 nm, compound **1** is also directly excited (Figure 8) but, as it is not fluorescent in aqueous media, the observation of compound fluorescence can only be due to the interaction between this thienopyridine and the proteins, either due to FRET from BSA/MDR1, or due to the compound location in hydrophobic protein domains.

For BSA, [protein]/[compound] ratios of 0.5:1, 1:1, 2:1 and 4:1 were investigated, corresponding to [amino acid]/[compound] ratios of 292:1, 583:1, 1166:1 and 2332:1, respectively, as BSA molecule has 583 amino acids (from which 20 tyrosines and 2 tryptophans per chain).[56]

Figure 9 shows the fluorescence emission of compound **1** in the presence of BSA at different pH values, for [BSA]/[**1**]=1. The ratio of emission intensities between the compound and protein is displayed at inset, as function of protein concentration for the several pH values. Compound emission is clearly higher at pH=7 (BSA in native form), especially at smaller protein concentrations. However, at pH=2, the fluorescence emission of the compound is not detected at any protein/compound ratio.

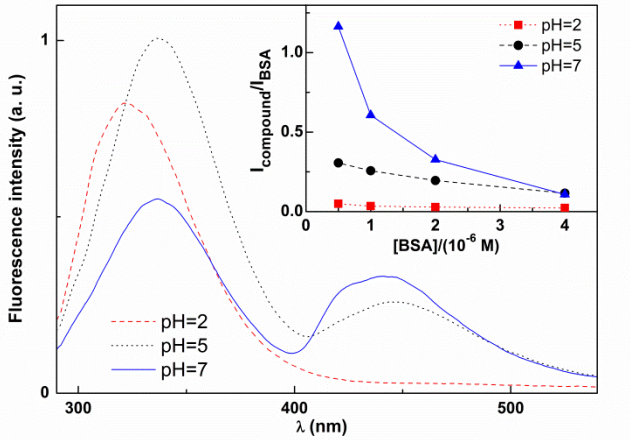

Fig. 9 Fluorescence spectra of BSA/compound solutions (λ_{exc} = 280 nm) at pH=2; 5; 7 for [BSA]/[compound]=1:1. Inset: Ratio of fluorescence intensities between compound and BSA as function of BSA concentration.

Figure 10 displays the excitation spectra, with the emission collected at compound fluorescence band (λ_{em}=450 nm) for [BSA]/[compound]=1, as an example. Excitation spectrum at pH=7 resembles the absorption spectrum of compound **1**, with additional bands of the amino acids that transfer their excitation energy to compound **1**. The excitation spectrum at pH=2 (Figure 10), showing a very low intensity, resembles the absorption spectrum of the compound with much less features of the amino acids absorption. This clearly indicates a very low energy transfer efficiency at pH=2. The interaction of this thienopyridine derivative with BSA is therefore conformation dependent, with a higher efficiency of energy transfer from BSA to compound at higher pH (BSA native form).

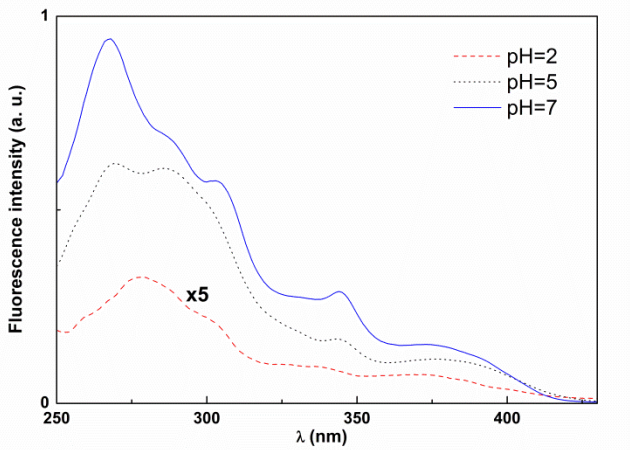

Fig. 10 Excitation spectra of BSA/compound solutions (λ_{em}=450 nm) at pH=2; 5; 7 for [BSA]/[compound]=1:1 ([compound]=1×10^{-6} M).

The interaction of compound **1** with the multidrug resistance protein MDR1 (1280 amino acids, with 72 tyrosines and 22

tryptophans per molecule[57]) was studied using several [MDR1]/[compound] ratios (corresponding to [amino acid]/[compound]=46, 92 and 184), keeping [compound] constant. Emission of compound **1** is detected for all ratios (decreasing at higher concentrations of protein), evidencing FRET from excited MDR1 to the thienopyridine derivative, which efficiency decreases with increasing protein concentration (Figure 11), as observed for BSA.

Using equations (5)-(8), the values of FRET efficiency, Förster radius and donor-acceptor distances were determined (Table 4). The donor integrated fluorescence intensity in the presence of acceptor (equation 5) was calculated from the emission of the protein in the presence of the drug, decomposing the total spectra in two components (protein emission and drug emission).

Comparing the FRET efficiencies of both systems, at approximately the same donor/acceptor, [Tyr+Trp]/[compound], ratio, it can be observed that Φ_{RET} values are significantly lower for the MDR1 protein, showing a stronger interaction of compound **1** with BSA. Donor-acceptor distances, r_{AD}, are also higher for MDR1 (Table 4).

Assuming that compound molecules distribute themselves randomly between the proteins, the probability of a subpopulation with a given number of compound molecules can be estimated using a Poisson distribution. The BSA entries in Table 4 correspond to mean occupation values of 1 and 0.5. The probabilities of having proteins with 0, 1, 2 and 3 compound molecules are, respectively, 0.37, 0.37, 0.18, 0.061 (for occupation value 1) and 0.61, 0.30, 0.076, 0.013 (for occupation value 0.5). The increase of subpopulation with no compound molecules results obviously in an overall decrease of energy transfer and an apparent increase in average donor-acceptor distance. The effect of the decrease in subpopulations with two or more compound molecules depends on the type of interaction of the compound with protein. If an interaction with a specific protein site occurs, no variation of energy transfer efficiency is expected. On the contrary, a random distribution of compound molecules within the protein would predict a decrease in energy transfer efficiency, as this value would then be higher in proteins with two or more compound molecules (decreased average donor-acceptor distance). The variation with more impact is the increase in the subpopulation without compound molecules in which energy transfer cannot occur. As a result and irrespective of the type of protein-compound interaction, the overall efficiency of energy transfer is expected to decrease with the increase of protein content and the consequent decrease of average compound occupation value.

The r_{AD} values for BSA at pH=5 and 7 (Table 4) are lower than the ones reported for the interaction of other drugs with serum albumins, namely the anticancer anastrozole,[17] phenylethanoid glycosides[59] and the flavonol morin.[60] This fact points to a high affinity of compound **1** to albumin, but not to MDR1. This high affinity indicates that serum albumin (in the native form) is able to bind and carry compound **1** in the blood stream. On the other hand, the low affinity to human MDR1 gives indication that the compound may not be expelled out of the cells by this type of membrane proteins (promoters of drug resistance).

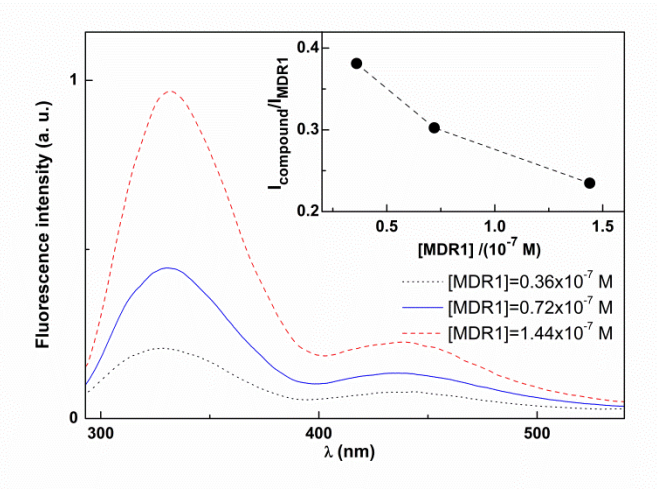

Fig. 11 Fluorescence spectra of MDR1/compound solutions (λ_{exc} = 280 nm) for several [MDR1]/[compound] ratios. Inset: Ratio of fluorescence intensities between compound and MDR1, as function of MDR1 concentration.

Table 4. FRET efficiencies (Φ_{RET}), Förster radius (R_0) and donor/acceptor distances (r_{AD}) for the interaction of compound **1** with BSA and MDR1.

Protein	pH	Φ_F of protein[a]	R_0 (nm)	[Tyr+Trp]/[**1**]	Φ_{RET}	r_{AD} (nm)
BSA	2	0.07	2.3	11:1	≈ 0	---
				22:1		
	5	0.17	2.6	11:1	0.21	3.3
				22:1	0.20	3.3
	7	0.13	2.5	11:1	0.74	2.1
				22:1	0.51	2.5
MDR1	7	0.16	2.6	7:1	0.15	3.5
				14:1	0.06	4.1

[a] Relative to *L*-Tryptophan in water, pH=7.2 (Φ_F=0.14 at 25 ºC).[58]

Drug resistance is one of the major problems in cancer chemotherapy. The results presented here are promising for future developments using this thienopyridine derivative as an antitumor drug.

Conclusions

The antitumor methyl 3-amino-6-(benzo[*d*]thiazol-2-ylamino)thieno[3,2-*b*]pyridine-2-carboxylate presents very reasonable fluorescence quantum yields and a solvent sensitive emission, except in protic solvents. The compound is also fluorescent in liposomes, and fluorescence anisotropy measurements indicate that it is mainly located in the lipid membrane, feeling an increase in fluidity above the melting temperature of lipids and by inclusion of cholesterol and DMPG in the membranes.

The lower affinity of this thienopyridine derivative for the multidrug resistance protein MDR1, when compared to BSA, is promising for the use of this compound as an antitumour drug, as MDR1 promotes drug resistance in cells. Furthermore, this hydrophobic compound can be transported in nanoliposomes in

future drug delivery applications, the Egg-PC:Ch (7:3), Egg-PC:Ch:DMPG (7:3:1) and DPPC:DMPG (1:2) formulations being the best for this compound, exhibiting low size and polydispersity.

Acknowledgements

Foundation for the Science and Technology (FCT, Portugal), FEDER/COMPETE and QREN for financial support to the Research Centres, CFUM [Strategic Project PEst-C/FIS/UI0607/2013 (FCOMP-01-0124-FEDER-022711) and CQ/UM [Strategic Project PEst-C/QUI/UI0686/2013 (FCOMP-01-0124-FEDER-022716)] and n-STeP Project NORTE-07-0124-FEDER-000039 supported by the Operational Regional Programme of North of Portugal (ON.2). FCT and POPH/QREN/FSE are acknowledged for the Post-Doc. grant of R.C.C. (SFRH/BPD/68344/2010).

Notes and references

1 I. Hayakama, R. Shioya, T. Agatsuma, H. Furokawa and Y. Sugano, Thienopyridine and benzofuran derivatives as potent anti-tumor agents possessing different structure-activity relationships, *Bioorg. Med. Chem.*, 2004, **14**, 3411-3414.

2 M.-J. R. P. Queiroz, R. C. Calhelha, L. Vale-Silva, E. Pinto and M. S.-J. Nascimento, Novel [6-(hetero)arylamino]thieno [3,2-*b*]pyridines: synthesis and antitumoral activities, *Eur. J. Med. Chem.*, 2010, **45**, 5732-5738.

3 M.-J. R. P. Queiroz, R. C. Calhelha, L. Vale-Silva, E. Pinto, R. T. Lima and M. H. Vasconcelos, Efficient synthesis of 6-(hetero)arylthieno[3,2-*b*]pyridines by Suzuki-Miyaura coupling. Evaluation of growth inhibition on human tumor cell lines, SARs and effects on the cell cycle, *Eur. J. Med. Chem.*, 2010, **46**, 5628-5634.

4 M.-J. R. P. Queiroz, R. C. Calhelha, L. Vale-Silva, E. Pinto, G. M. Almeida and M. H. Vasconcelos, Synthesis and evaluation of tumor cell growth inhibition of methyl 3-amino-6-[(hetero)arylethynyl]thieno[3,2-*b*]pyridine-2-carboxylates. Structure-activity relationships, effects on the cell cycle and apoptosis, *Eur. J. Med. Chem.*, 2011, **46**, 236-240.

5 M.-J. R. P. Queiroz, D. Peixoto, R. C. Calhelha, P. Soares, T. Santos, R. T. Lima, J. F. Campos, R. M. V. Abreu, I. C. F. R. Ferreira and M. H. Vasconcelos, New di(hetero)arylethers and di(hetero)arylamines in the thieno[3,2-*b*]pyridine series: Synthesis, growth inhibitory activity on human tumor cell lines and non-tumor cells, effects on cell cycle and on programmed cell death, *Eur. J. Med. Chem.*, 2013, **69**, 855-862.

6 D. H. Boschelli, B. Wu, A. C. B. Sosa, H. Durutlic, J. J. Chen, Y. Wang, J. M. Golas, J. Lucas and F. Boschelli, Synthesis and Src Kinase Inhibitory Activity of 2-Phenyl- and 2-Thienyl-7-phenylaminothieno[3,2-*b*]pyridine-6-carbonitriles, *J. Med. Chem.*, 2005, **48**, 3891-3902.

7 H. Heyman, R. Frey, P. Bousquet, G. Cunha, M. Moskey, A. Ahmed, N. Soni, P. Marcotte, L. Pease, K. Glaser, M. Yates, J. Bouska, D. Albert, C. B. Schaefer, P. Dandliker, K. Stewart, P. Rafferty, S. Davidsen, M. Michaelides and M. Curtin, Thienopyridine urea inhibitors of KDR kinase, *Bioorg. Med. Chem. Lett*., 2007, **17**, 1246-1249.

8 M. J. Munchhof, J. S. Beebe, J. M. Casavant, B. A. Cooper, J. L. Doty, R. C. Hidgon, S. M. Hillerman, C. I. Doderstrom, E. A. Knauth, M. A. Marx, A. M. K. Rossi, S. B. Sobolov, and J. Sun, Design and SAR of thienopyrimidine and thienopyridine inhibitors of VEGFR-2 kinase activity, *Bioorg. Med. Chem. Lett.*, 2004, **14**, 21-24.

9 S. Claridge, F. Raeppel, M.-C. Granger, N. Bernstein, O. Saavedra, L. Zhan, D. Llewellyn, A. Wahhab, R. Deziel, J. Rahil, N. Beaulieu, H. Nguyen, I. Dupont, A. Barsalou, C. Beaulieu, I. Chute, S. Gravel, M.-F. Robert, S. Lefebvre, M. Dubay, R. Pascal, J. Gillespie, Z. Jin, J. Wang, J. M. Besterman, A. R. MacLeod, and A. Vaisburg, Discovery of a novel and potent series of thieno[3,2-*b*]pyridine-based inhibitors of c-Met and VEGFR-2 tyrosine kinases, *Bioorg. Med. Chem. Lett.*, 2008, **18**, 2793-2798.

10 C. Sánchez, A. Mercado, H. Conteras, P. Mendoza, J. Cabezas, C. Acevedo, C. Huidobro and E. A. Castellón, Chemotherapy sensitivity recovery of prostate cancer cells by functional inhibition and knock down of multidrug resistance proteins, *Prostate*, 2011, **71**, 1810-1817.

11 N. Kahya, E. Pécheur, W. P. Boeij, D. A. Wiersma and D. Hoekstra, Reconstitution of membrane proteins into giant unilamellar vesicles via peptide-induced fusion, *Biophys. J.*, 2001, **81**, 1464-1474.

12 P. Curnow, M. Lorch, K. Charalambous and P.J. Booth, The Reconstitution and Activity of the Small Multidrug Transporter EmrE is Modulated by Non-bilayer Lipid Composition, *J. Mol. Biol.*, 2004, **343**, 213-222.

13 N. Wang, L. Ye, B. Q. Zhao and J. X. Yu, Spectroscopic studies on the interaction of efonidipine with bovine serum albumin, *Braz. J. Med. Biol. Res.*, 2008, **41**, 589-595.

14 B. Mishra, A. Barik, K. I. Priyadarsini and H. Mohan, Fluorescence spectroscopic studies on binding of a flavonoid antioxidant quercetin to serum albumins, *J. Chem. Sci.*, 2005, **117**, 641-647.

15 Q. Yue, T. Shen, C. Wang, C. Gao and J. Liu, Study on the Interaction of Bovine Serum Albumin with Ceftriaxone and the Inhibition Effect of Zinc (II), *Int. J. Spectroscopy*, 2012, Article ID 284173.

16 M. Sarkar, S. S. Paul and K. K. Mukherjea, Interaction of bovine serum albumin with a psychotropic drug alprazolam: Physicochemical, photophysical and molecular docking studies, *J. Lumin*., 2013, **142**, 220-230.

17 R. Punith and J. Seetharamappa, Spectral characterization of the binding and conformational changes of serum albumins upon interaction with an anticancer drug, anastrozole, *Spectroc. Acta A – Molec. Biomolec. Spectr.*, 2012, **92**, 37-41.

18 X. M. He and D. C. Carter, Atomic structure and chemistry of human serum albumin, *Nature*, 1992, **358**, 209-215.

19 S. Sugio, A. Kashima, S. Mochizuki, M. Noda and K. Kobayashi, Crystal structure of human serum albumin at 2.5 Å resolution, *Protein Eng.*, 1999, **12**, 439-446.

20 E. M. Nagy, C. Nardon, L. Giovagnini, L. Marchiò, A. Trevisan, D. Fregona, Promising anticancer mono- and dinuclear ruthenium(III) dithiocarbamato complexes: systematic solution studies", *Dalton Trans.*, 2011, **40**, 11885-11895.

21 K. A. Majorek, P. J. Porebski, A. Dayal, M. D. Zimmerman, K. Jablonska, A. J. Stewart, M. Chruszcz, and W. Minor, Structural and immunologic characterization of bovine, horse, and rabbit serum albumins, *Mol. Immun.*, 2012, **52**, 174-182.

22 Y. Malam, M. Loizidou and A. Seifalian, Liposomes and nanoparticles: nanosized vehicles for drug delivery in cancer, *Trends Pharmacol. Sci.*, 2009, **30**, 592-599.

23 R. Banerjee, Liposomes: applications in medicine, *J. Biomater. Appl.*, 2001, **16**, 3-21.

24 K. A. Riske, L. Q. Amaral, H.-G. Döbereiner and M. T. Lamy, Mesoscopic structure in the chain-melting regime of anionic phospholipid vesicles: DMPG, *Biophys. J*., 2004, **8**6, 3722-3733.

25 R. P. Barroso, K. R. Perez, I. M. Cuccovia and M. T. Lamy, Aqueous dispersions of DMPG in low salt contain leaky vesicles, *Chem. Phys. Lipids*, 2012, **165**, 169-177.

26 Y. Ran and S. H. Yalkowsky, Halothane, a novel solvent for the preparation of liposomes containing 2-4'-amino-3'-methylphenyl benzothiazole (AMPB), an anticancer drug: A technical note, *AAPS Pharm. Sci. Tech*., 2003, **4**, 70-74.

27 D. Perrin and B. Dempsey, *Buffers for pH and Metal Ion Control*, Chapman and Hall, London, 1974.

28 S. Batzri and E. Korn, Single bilayer liposomes prepared without sonication, *Biophys. Biochim. Acta – Biomembranes*, 1973, **298**, 1015-1019.

29 J. Kremer, M. Esker, C. Pathmamanoharan and P. Wiersema, Vesicles of variable diameter prepared by a modified injection method, *Biochemistry*, 1977, **16**, 3932-3935.
30 B. R. Lentz, Membrane "fluidity" as detected by diphenylhexatriene probes, *Chem. Phys. Lipids*, 1989, **50**, 171-190.
31 J. S. Vincent, S. D. Revak, C. D. Cochrane and I. W. Levin, Interactions of model human pulmonary surfactants with a mixed phospholipid bilayer assembly: Raman spectroscopic studies, *Biochemistry*, 1993, **32**, 8228-8238.
32 M. T. Lamy-Freund and K. A. Riske, The peculiar thermo-structural behavior of the anionic lipid DMPG, *Chem. Phys. Lipids*, 2003, **122**, 19-32.
33 E. Feitosa, P. Barreleiro and G. Olofsson, Phase transition in dioctadecyldimethylammonium bromide and chloride vesicles prepared by different methods, *Chem. Phys. Lipids*, 2000, **105**, 201-213.
34 S. Fery-Forgues and D. Lavabre, Are fluorescence quantum yields so tricky to measure? A demonstration using familiar stationery products, *J. Chem. Educ*., 1999, **76**, 1260-1264.
35 J. N. Demas and G. A. Crosby, Measurement of photoluminescence quantum yields – Review, *J. Phys. Chem.*, 1971, **75**, 991-1024.
36 D. Eaton, Reference materials for fluorescence measurement, *Pure & Appl. Chem*., 1988, **60**, 1107-1114.
37 S. R. Meech and D. Phillips, Photophysics of some common fluorescence standards, *J. Photochem.*, 1983, **23**, 193-217.
38 J. R. Lakowicz, *Principles of Fluorescence Spectroscopy*, 3rd Edition, Springer, New York, 2006.
39 N. Mataga and T. Kubota, *Molecular Interactions and Electronic Spectra*, Marcel Dekker, New York, 1970.
40 B. Valeur, *Molecular Fluorescence – Principles and Applications*, Wiley-VCH, Weinheim, 2002.
41 M.-J. R. P. Queiroz, S. Dias, D. Peixoto, A. R. O. Rodrigues, A. D. S. Oliveira, P. J. G. Coutinho, L. A. Vale-Silva, E. Pinto, and E. M. S. Castanheira, New potential antitumoral di(hetero)arylether derivatives in the thieno[3,2-*b*]pyridine series: Synthesis and fluorescence studies in solution and in nanoliposomes, *J. Photochem. Photobiol. A: Chem*., 2012, **238**, 71-80.
42 M.-J. R. P. Queiroz, D. Peixoto, A. R. O. Rodrigues, P. Mendes, C. N. C. Costa, P. J. G. Coutinho and E. M. S. Castanheira, New 1,3-diarylureas linked by C-C Suzuki coupling to the methyl 3-aminothieno[3,2-*b*]pyridine-2-carboxylate moiety: synthesis and fluorescence studies in solution and in lipid membranes, *J. Photochem. Photobiol. A: Chem*., 2013, **255**, 27-35.
43 M. S. D. Carvalho, A. C. L. Hortelão, R. C. Calhelha, A. S. Abreu, P. J. G. Coutinho, M.-J. R. P. Queiroz and E. M. S. Castanheira, Fluorescence studies on potential antitumor 6-(hetero)arylthieno[3,2-*b*]pyridine derivatives in solution and in nanoliposomes, *J. Photochem. Photobiol. A: Chem*. 2013, **264**, 56-66.
44 N. J. Turro, J. C. Scaiano and V. Ramamurthy, *Modern Molecular Photochemistry of Organic Molecules*, University Science Books, Sausalito (California), 2009.
45 D. R. Lide (Ed.), *Handbook of Chemistry and Physics*, 83th Edition, CRC Press, Boca Raton, 2002.
46 *Gaussian 09, Revision A.02*, M. J. Frisch, G. W. Trucks, H. B. Schlegel, G. E. Scuseria, M. A. Robb, J. R. Cheeseman, G. Scalmani, V. Barone, B. Mennucci, G. A. Petersson, H. Nakatsuji, M. Caricato, X. Li, H. P. Hratchian, A. F. Izmaylov, J. Bloino, G. Zheng, J. L. Sonnenberg, M. Hada, M. Ehara, K. Toyota, R. Fukuda, J. Hasegawa, M. Ishida, T. Nakajima, Y. Honda, O. Kitao, H. Nakai, T. Vreven, J. A. Montgomery, Jr., J. E. Peralta, F. Ogliaro, M. Bearpark, J. J. Heyd, E. Brothers, K. N. Kudin, V. N. Staroverov, R. Kobayashi, J. Normand, K. Raghavachari, A. Rendell, J. C. Burant, S. S. Iyengar, J. Tomasi, M. Cossi, N. Rega, J. M. Millam, M. Klene, J. E. Knox, J. B. Cross, V. Bakken, C. Adamo, J. Jaramillo, R. Gomperts, R. E. Stratmann, O. Yazyev, A. J. Austin, R. Cammi, C. Pomelli, J. W. Ochterski, R. L. Martin, K. Morokuma, V. G. Zakrzewski, G. A. Voth, P. Salvador, J. J. Dannenberg, S. Dapprich, A. D. Daniels, Ö. Farkas, J. B. Foresman, J. V. Ortiz, J. Cioslowski and D. J. Fox, Gaussian, Inc., Wallingford CT, 2009.
47 F. Jensen, *Introduction to Computational Chemistry*, John Wiley & Sons, West Sussex, England, 1999.
48 T. Le Bahers, C. Adamo and I. Ciofini, A Qualitative Index of Spatial Extent in Charge-Transfer Excitations, *J. Chem. Theory Comput*. 2011, **7**, 2498-2506.
49 L. Tian and C. Feiwu, Multiwfn: A multifunctional wavefunction analyser, *J. Comput. Chem*. 2012, **33**, 580-592.
50 A. S. Abreu, E. M. S. Castanheira, Maria-João R. P. Queiroz, Paula M. T. Ferreira, L. A. Vale-Silva and E. Pinto, Nanoliposomes for encapsulation and delivery of the potential antitumoral methyl 6-methoxy-3-(4-methoxyphenyl)-1*H*-indole-2-carboxylate, *Nanoscale Res. Lett.*, 2011, **6**, article 482.
51 D. Papahadjopoulos and N. Miller, Phospholipid model membranes. I. Structural characteristics of hydrated liquid crystals, *Biochim. Biophys. Acta*, 1967, **135**, 624-638.
52 S. J. Strickler and R. A. Berg, Relationship between absorption intensity and fluorescence lifetime of molecules, *J. Chem. Phys.*, 1962, **37**, 814.
53 J. N. Israelachvili, S. Marcelja and R. G. Horn, Physical principles of membrane organization, *Q. Rev. Biophys.* 1980, **13**, 121-200.
54 D. B. Kell and C. M. Harris, On the dielectrically observable consequences of the diffusional motions of lipids and proteins in membranes. 1. Theory and overview, *Eur. Biophys. J.*, 1985, **12**, 181-197.
55 C. T. Lee Jr., K. A. Smith and T. A. Hatton, Photocontrol of protein folding: the interaction of photosensitive surfactants with bovine serum albumin, *Biochemistry*, 2005, **44**, 524-536.
56 K. Hirayama, S. Akashi, M. Furuya and K. I. Fukuhara, Rapid confirmation and revision of the primary structure of bovine serum albumin by ESIMS and Frit-FAB LC/MS, *Biochem. Biophys. Res. Commun.*, 1990, **173**, 639-646.
57 J. M. Walker (Ed.), *The Proteomics Protocols Handbook*, Humana Press, New York, 2005.
58 E. P. Kirby and R. F. Steiner, Influence of solvent and temperature upon the fluorescence of indole derivatives, *J. Phys. Chem.*, 1970, **74**, 4480-4490.
59 A.-Z. Wu, C.-Z. Lin, Y.-J. Zhai, J.-L. Zhuo and C.-C. Zhu, Investigation of the interaction between two phenylethanoid glycosides and bovine serum albumin by spectroscopic methods, *J. Pharm. Anal.*, 2013, **3**, 61-65.
60 Z.-d. Qi, Y. Zhang, F.-l. Liao, Y-w. Ou-Yang, Y. Liu and X. Yang, Probing the binding of morin to human serum albumin by optical spectroscopy, *J. Pharm. Biomed. Anal.*, 2008, **46**, 699-706.

